

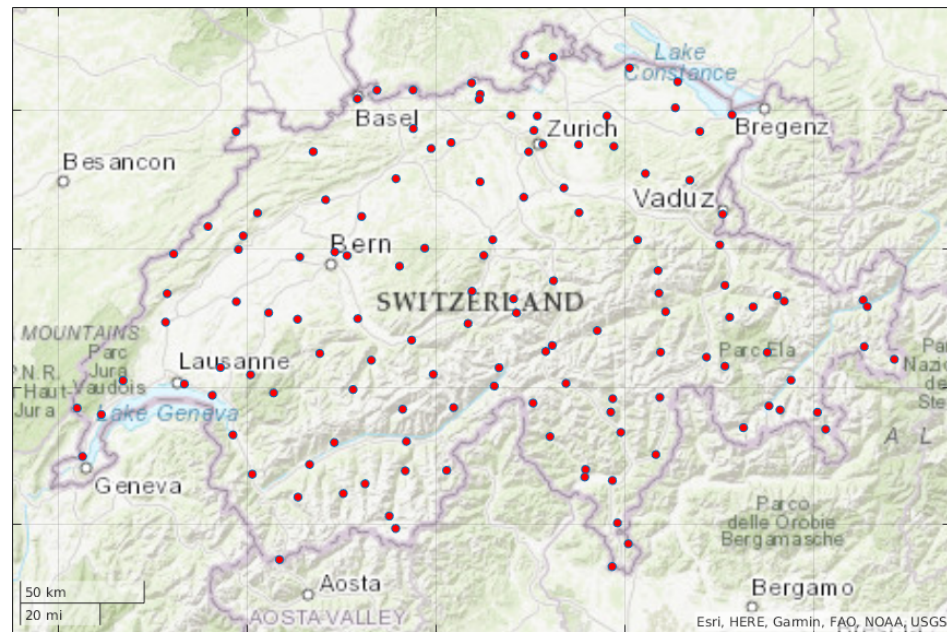


# Solar Panel Project

Optimization of Photovoltaic Park Location in Switzerland

Perle Boucard  
Agathe Gaudillat

EPFL – Computational methods and tools Project  
December 2025



# Contents

<b>1 Deviations from Project Proposal</b>	<b>2</b>
<b>2 Introduction to the Problem</b>	<b>2</b>
2.1 Motivations and Research Question . . . . .	2
2.2 Project Objectives . . . . .	2
2.3 Project Content . . . . .	2
2.4 Scope Exclusions and Resulting Limitations . . . . .	3
2.5 Envisioned Scenarios . . . . .	3
<b>3 Approach Used</b>	<b>3</b>
3.1 General Nature of the Model . . . . .	3
3.2 Data Preprocessing and Selection . . . . .	4
3.3 Sunshine Stability and Optimal Trade-off . . . . .	4
3.4 Modeling the Irradiance in the Module Plane . . . . .	5
3.5 Cell Temperature Model . . . . .	5
3.6 Photovoltaic Efficiency Model . . . . .	6
3.7 Numerical Implementation and Optimization . . . . .	7
<b>4 Feasibility and Site Context</b>	<b>7</b>
4.1 Accessibility . . . . .	7
4.2 Topography . . . . .	7
4.3 Existing Infrastructure . . . . .	7
4.4 Urbanization and Land-Use Constraints . . . . .	7
4.5 System-Level Losses (Discussion) . . . . .	8
<b>5 Results</b>	<b>8</b>
5.1 Comparative Analysis of Solar Exposure . . . . .	8
5.2 Sunshine Stability and Optimal Trade-off . . . . .	10
5.3 Photovoltaic Cell Temperature . . . . .	11
5.4 Panel Efficiency and Thermal Effects . . . . .	12
<b>6 Conclusion and outlook</b>	<b>12</b>
<b>7 Authorship Statement</b>	<b>13</b>
<b>References</b>	<b>13</b>
<b>Appendices</b>	<b>15</b>
<b>A Structure of the Input Data</b>	<b>15</b>
<b>B Example of the EPOA_table Structure</b>	<b>15</b>
<b>C Photovoltaic Technologies Overview</b>	<b>15</b>
<b>D Station Abbreviations and Full Names</b>	<b>16</b>
<b>E Maps for the Photovoltaic Panel Location</b>	<b>17</b>

# 1 Deviations from Project Proposal

In the project proposal, we indicated that several years of data would be analyzed, without specifying the exact period. The final analysis was conducted for the years 2022, 2023, and 2024, based on data availability and completeness.

The planned schedule was largely respected, particularly for site validation and comparison. Although the proposal mentioned the end of November as a deadline, these tasks were completed by mid-November.

The time required for documenting the codebase, preparing the GitHub repository, and writing the final report was underestimated in the proposal. These activities were therefore carried out between early December and December 17.

Finally, while the proposal initially considered evaluating multiple environmental parameters affecting photovoltaic yield, the final study focuses primarily on cell temperature. This choice allowed a more detailed and consistent analysis of thermal effects. The mathematical formulations used remain consistent with those presented in the proposal, although notation and terminology were slightly refined.

## 2 Introduction to the Problem

### 2.1 Motivations and Research Question

Renewable energy plays a central role in reducing dependence on fossil fuels and mitigating climate change [1]. Among renewable sources, solar energy is particularly attractive due to its wide availability, modularity, and technological maturity. As photovoltaic (PV) installations expand, identifying locations that maximize energy yield while remaining technically and economically feasible has become a key challenge.

In this context, our client, a Swiss energy company, seeks to identify optimal locations for new photovoltaic parks in Switzerland. The objective is not only to maximize solar exposure, but also to assess how local environmental conditions influence photovoltaic performance, thereby supporting informed decision-making for large-scale deployment.

### 2.2 Project Objectives

The objective of this project is to compare several potential sites in Switzerland based on their solar exposure and the resulting photovoltaic performance. In particular, we analyze both sunshine duration and temperature-dependent photovoltaic yield in order to identify locations offering favorable conditions for a large-scale photovoltaic park.

Monocrystalline silicon technology was selected for this study, as it currently represents the dominant photovoltaic technology worldwide, accounting for approximately 80–90% of installed capacity [2]. Its high efficiency, technological maturity, and favorable cost-to-performance ratio make it well suited for utility-scale installations.

### 2.3 Project Content

This project will include :

- Analysis of sunlight duration (sunshine hours) for several stations in Switzerland;
- Calculation of the average temperature of the cells:
  - By estimating the Effective Plane of Array (effective irradiance on the plane of orientation, EPOA),
  - From wind speed data;
- Estimation of panel yield based on cell temperature;
- Comparison of sites based on:
  - Their sunlight duration,
  - The yield impacted by the estimated cell temperature.

## 2.4 Scope Exclusions and Resulting Limitations

To clarify the link between the processes excluded from the project and the resulting limitations of the analysis, we summarize them below:

- **Meteorological factors**

- Excluded: humidity, precipitation, detailed cloud cover, albedo.
  - Limitation: these parameters can significantly affect PV yield, especially in alpine environments, but were not modeled.

- **Electrical and system-related**

- Excluded: modeling of electrical losses.
  - Limitation: the resulting yields may slightly overestimate real performance.

- **Simplified system configuration**

- Excluded: variations in orientation or tilt; no tracking systems.
  - Limitation: results are restricted to a fixed-tilt configuration and do not reflect potential performance optimization.

- **Data and model**

- Limitation (not from exclusions): use of empirical irradiance and temperature models that miss micro-climatic effects.
  - Limitation (not from exclusions): use of monthly-averaged data smoothing short-term variability.

## 2.5 Envisioned Scenarios

To compare the Swiss stations, we will consider the study of sunlight duration and cell yield for 2022, 2023, and 2024.

We use data from MeteoSuisse [4], such as solar radiation, irradiance and temperature, to analyses the duration of sunshine over several years and to estimate the potential output of the park.

# 3 Approach Used

## 3.1 General Nature of the Model

The approach used in this project is mainly empirical. It is based on sunshine duration time series from 132 meteorological stations across Switzerland [4]. The data are provided as monthly CSV files and include, for each station, geographical coordinates, altitude, and several meteorological variables (air temperature, wind speed, global solar radiation, etc.). An illustrative excerpt of the raw monthly CSV meteorological data structure is provided in Appendix A (Figure 5).

Using these measurements, we apply well-established formulas from the literature to convert global horizontal irradiance into plane-of-array irradiance (Eq. (4)) and to estimate the photovoltaic cell temperature (Eq. (8)) [5, 6]. The equations linking irradiance, cell temperature, and PV efficiency are therefore standard and documented in published work, while the input values come directly from actual station observations.

The main objective is to compare the different sites in terms of efficiency and sunshine duration. The model is therefore used to analyze the influence of cell temperature and location on efficiency, and to rank the stations accordingly.

### 3.2 Data Preprocessing and Selection

The first step in the analysis is to clean and structure the raw meteorological data. We have implemented a function called `function_clean_data` in MATLAB which, for each station:

- scans all monthly CSV files in the `donnees_mensuelles` directory,
- extracts the years 2022, 2023, and 2024 for each station,
- retains only the columns required for our analysis:
  - `tre005m0`: air temperature at 5 cm, expressed in °C;
  - `fk1010m0`: wind speed at 10 m, expressed in m/s;
  - `gre000m0`: global horizontal irradiance (GHI), provided as a monthly mean value in  $\text{W m}^{-2}$ ;
  - `sre000m0`, `sremaxmv`: variables related to sunshine duration in minutes and %.
- removes any station for which at least one of these variables contains missing values (`NaN`).

Out of the 132 initial stations, only those with complete time series over the full three-year period are retained, resulting in a total of 63 stations (see Appendix D). This ensures that efficiency comparisons are not affected by measurement gaps.

From these cleaned tables, we calculated the annual sunshine durations by doing the sum of each monthly values and represented them in a bar chart (see Results, subsection 5.1)

In addition to total sunshine duration, a stability analysis based on monthly variability was performed to evaluate the robustness of solar exposure throughout the year (see Results, subsection 5.2).

### 3.3 Sunshine Stability and Optimal Trade-off

Beyond total sunshine duration, the temporal distribution of solar exposure over the year influences the reliability and predictability of photovoltaic energy production. Stations with similar annual sunshine totals may exhibit markedly different seasonal patterns, leading to different production profiles.

To quantify this effect, an intra-annual stability analysis of sunshine duration was performed for each station and each year (2022–2024). Monthly sunshine duration values were used to compute:

- the annual mean sunshine duration  $\mu_{\text{annual}}$ ,
- the standard deviation of the monthly values  $\sigma_{\text{monthly}}$ ,
- the coefficient of variation (CV), defined as:

$$\text{CV} = \frac{\sigma_{\text{monthly}}}{\mu_{\text{annual}}} \quad (1)$$

The coefficient of variation provides a normalized measure of seasonal variability, with lower values indicating a more homogeneous distribution of sunshine throughout the year.

In addition to ranking stations according to their CV, a trade-off metric was defined to identify locations combining high solar potential and low variability:

$$\text{Score} = \frac{\mu_{\text{annual}}}{\text{CV}} \quad (2)$$

This metric favors stations offering both high annual sunshine duration and stable intra-annual exposure. The application and interpretation of these indicators are presented in the Results section (Subsection E).

### 3.4 Modeling the Irradiance in the Module Plane

The next step is to convert the cleaned global horizontal irradiance (GHI) data into plane-of-array irradiance ( $E_{\text{POA}}$ ). This part relies on the PVlib library for MATLAB [7].

The monthly global horizontal irradiance is decomposed into direct and diffuse components according to [5]:

$$\text{GHI} = \text{DNI} \cdot \cos(\theta_z) + \text{DHI}, \quad (3)$$

where DNI is the direct normal irradiance, DHI is the diffuse horizontal irradiance, and  $\theta_z$  is the solar zenith angle.

The plane-of-array irradiance is then computed as the sum of three components [5]:

$$E_{\text{POA}} = G_{\text{beam}} + G_{\text{sky\_diffuse}} + G_{\text{ground}}, \quad (4)$$

with:

- direct component on the tilted plane:

$$G_{\text{beam}} = \text{DNI} \cdot \max(0, \cos(\theta_i)), \quad (5)$$

where  $\theta_i$  is the incidence angle, computed from latitude, longitude, date, tilt  $\beta$ , and azimuth  $\gamma$ ;

- diffuse sky component (isotropic model):

$$G_{\text{sky\_diffuse}} = \text{DHI} \cdot \frac{1 + \cos(\beta)}{2}; \quad (6)$$

- ground-reflected component (albedo  $\rho$ ):

$$G_{\text{ground}} = \rho \cdot \text{GHI} \cdot \frac{1 - \cos(\beta)}{2}. \quad (7)$$

In `function_EPOA`, we use a standard configuration (tilt  $\beta = 30^\circ$ , azimuth  $\gamma = 180^\circ$  for south-facing orientation, average albedo  $\rho = 0.2$ ) and rely on PVlib functions (`pvl_maketimestruct`, `pvl_spa`, `pvl_ephemeris`, `pvl_disc`, etc.) to:

1. compute the solar position (zenith and azimuth) for each timestamp;
2. estimate DNI and DHI from the GHI;
3. compute hourly  $E_{\text{POA}}$ , then convert these values into monthly energy ( $\text{kWh}/\text{m}^2/\text{month}$ ) and an annual average for each station.

All irradiance quantities involved in the above equations are expressed in  $\text{W m}^{-2}$ . In the present study, these values correspond to monthly mean irradiance levels. The monthly mean plane-of-array irradiance is converted into monthly energy values expressed in  $\text{kWh}, \text{m}^{-2}, \text{month}^{-1}$  by multiplying by the number of hours in each month.

The output of this step is an `EPOA_table` containing the twelve monthly energy values and their annual average for each station. An illustrative excerpt for the year 2024 is provided in Appendix B.

### 3.5 Cell Temperature Model

The operating temperature of the photovoltaic cells has a significant impact on the module efficiency. The cell temperature is estimated using the empirical model proposed by Faiman [6]:

$$T_{\text{cell}} = T_a + \frac{E_{\text{POA}}}{U_0 + U_1 \times WS}, \quad (8)$$

where  $T_a$  is the air temperature ( $^\circ\text{C}$ ),  $E_{\text{POA}}$  is the plane-of-array irradiance ( $\text{W}/\text{m}^2$ ),  $WS$  is the wind speed ( $\text{m}/\text{s}$ ), and  $U_0$ ,  $U_1$  are heat transfer coefficients ( $\text{W}/\text{m}^2\text{K}$  and  $\text{W}/\text{m}^3\text{sK}$ ).

Typical values measured by Faiman for glass-covered modules with Tedlar® back-sheet are:

- $U_0 \approx 25 \text{ W/m}^2\text{K}$ ,
- $U_1 \approx 6.84 \text{ W/m}^3\text{sK}$ .

In `function_Tcell`, we combine for each station:

- the monthly air temperatures (`tre005m0`),
- the average wind speeds (`fk1010m0`),
- the monthly  $E_{\text{POA}}$  values ( $\text{kWh/m}^2/\text{month}$ ) from `EPOA_table`,

to estimate the monthly mean cell temperature. A yearly average  $T_{\text{cell}}$  is then calculated and used as input for the efficiency model. An illustrative excerpt of the resulting `Tcell_2022` is presented in the Results section (Subsection 5.3, Figure 4).

The Faiman model was originally formulated for instantaneous operating conditions. In the present study, it is applied to monthly-averaged meteorological data (irradiance, air temperature, and wind speed). This approximation implicitly assumes that the nonlinear effects introduced by short-term variability are smoothed over monthly time scales.

While this approach may slightly underestimate peak cell temperatures during extreme conditions, it remains appropriate for comparative and long-term energy assessments, which are the primary focus of this study. Since the same averaging methodology is applied consistently across all stations, relative comparisons between locations are not affected.

### 3.6 Photovoltaic Efficiency Model

The instantaneous module efficiency is approximated by [8]:

$$\eta(T) = \eta_{\text{ref}} [1 - \beta (T_{\text{cell}} - T_{\text{ref}})], \quad (9)$$

where:

- $\eta_{\text{ref}}$  is the nominal efficiency at the reference temperature  $T_{\text{ref}} = 25^\circ\text{C}$ ,
- $\beta$  is the temperature coefficient (approximately  $0.004\text{--}0.005/\text{ }^\circ\text{C}$  for crystalline silicon),
- $T_{\text{cell}}$  is the estimated cell temperature.

Typical module efficiencies under standard test conditions (STC) for different technologies are listed in Table 1, based on [9]:

Cell Technology	Typical Efficiency (%)
Amorphous silicon (a-Si)	6–9
Polycrystalline silicon	13–18
Monocrystalline silicon (PERC, TOPCon)	18–24
Hetero junction / Tandem (HJT, Perovskite-Si)	25–28

Table 1: Typical PV module efficiencies under STC.

In our study, we focus on mono crystalline silicon (more information in appendix C) modules and use the average efficiency from the corresponding range as  $\eta_{\text{ref}}$ . Based on the estimated cell temperature and the plane-of-array irradiance, the electrical power produced by a photovoltaic module of surface area  $A$  is expressed as [10]:

$$P = \eta(T_{\text{cell}}) E_{\text{POA}} A, \quad (10)$$

To provide an order-of-magnitude estimate of the total energy production, a minimum photovoltaic park surface area of 2 hectares is assumed, corresponding to

$$A_{\text{park}} = 20,000 \text{ m}^2.$$

This surface represents the effective module area and is kept constant for all stations in order to enable a fair comparison between locations. Effects related to row spacing, mutual shading, and auxiliary infrastructure are not explicitly modeled and are therefore implicitly included in this effective area assumption. The resulting efficiency values are presented and analyzed in the Results section, Subsection 5.4.

### 3.7 Numerical Implementation and Optimization

The entire processing chain is implemented in MATLAB R2025a. The PVlib library is used for:

- generating time structures and solar angles,
- decomposing GHI into DNI and DHI,
- computing the irradiance in the module plane.

For the most computationally intensive part, ranking the stations based on efficiency and power, we developed a C function compiled as a MEX file (`pv_efficiency.c`). This function:

- receives the mean cell temperatures and station names as inputs,
- applies the efficiency model  $\eta(T)$  for each station,
- computes the corresponding electrical power assuming a reference irradiance,
- sorts the stations by decreasing efficiency,
- returns the sorted vectors to MATLAB and simultaneously exports the results to a CSV file.

This hybrid MATLAB/C architecture combines MATLAB's readability and plotting/report-generation capabilities with the speed of C for intensive loops and file handling.

## 4 Feasibility and Site Context

While solar potential is primarily determined by irradiance and temperature, the practical deployment of photovoltaic systems also depends on several site-specific constraints. These contextual factors are not included in the quantitative modeling but remain essential for interpreting the overall suitability of each location.

### 4.1 Accessibility

The ease of accessing the site affects transportation of equipment, construction operations, and long-term maintenance. Remote alpine areas may exhibit excellent solar potential but require significant logistical efforts.

### 4.2 Topography

Steep or unstable terrain can complicate installation, increase construction costs, or limit available surface area. In contrast, gently sloped or naturally flat locations are more suitable for large-scale PV deployment.

### 4.3 Existing Infrastructure

Proximity to power lines and sufficient grid capacity are key to integrating new PV installations. Sites far from electrical infrastructure may require costly grid extensions.

### 4.4 Urbanization and Land-Use Constraints

In densely built or highly regulated zones, land availability can be limited. Building-integrated PV may be possible, but ground-mounted installations can face permitting constraints or conflicts with existing activities.

## 4.5 System-Level Losses (Discussion)

In practical photovoltaic systems, additional losses occur beyond the module efficiency model. These include soiling, shading, snow cover, electrical mismatch, wiring and connection losses, inverter efficiency, light-induced degradation (LID), system ageing, and operational availability.

Tools such as PVWatts, a widely used photovoltaic performance calculator developed by the National Renewable Energy Laboratory (NREL), account for these effects using empirical loss factors applied to DC energy, i.e. the electrical energy produced by the PV modules before conversion to AC by the inverter. Under default assumptions, the total system loss is computed multiplicatively from individual loss mechanisms and typically amounts to approximately 14 % [11].

In this study, system-level losses were not explicitly modeled. The objective was to perform a relative comparison between potential sites under identical assumptions, focusing on irradiance and temperature-related effects. Applying uniform system losses would reduce absolute energy yields but would not affect the relative ranking of the sites.

## 5 Results

### 5.1 Comparative Analysis of Solar Exposure

For the analysis of the sunshine rate, we immediately observe that the sunniest location is Locarno (OTL), with between 10,313 and 12,887 hours of sunshine depending on the year. In contrast, Elm (ELM) is the least sunny station among those considered, with a sunshine duration almost half that of Locarno. These results highlight pronounced spatial variability in solar exposure, even within a relatively small geographic area.

These results are illustrated in Figure 1 (Figures 1a, 1b and 1c) below, corresponding to the years 2022, 2023 and 2024. The graphs were obtained using the implementation of our MATLAB code presented earlier, allowing a clear visualization of the differences in sunshine rates between the stations.

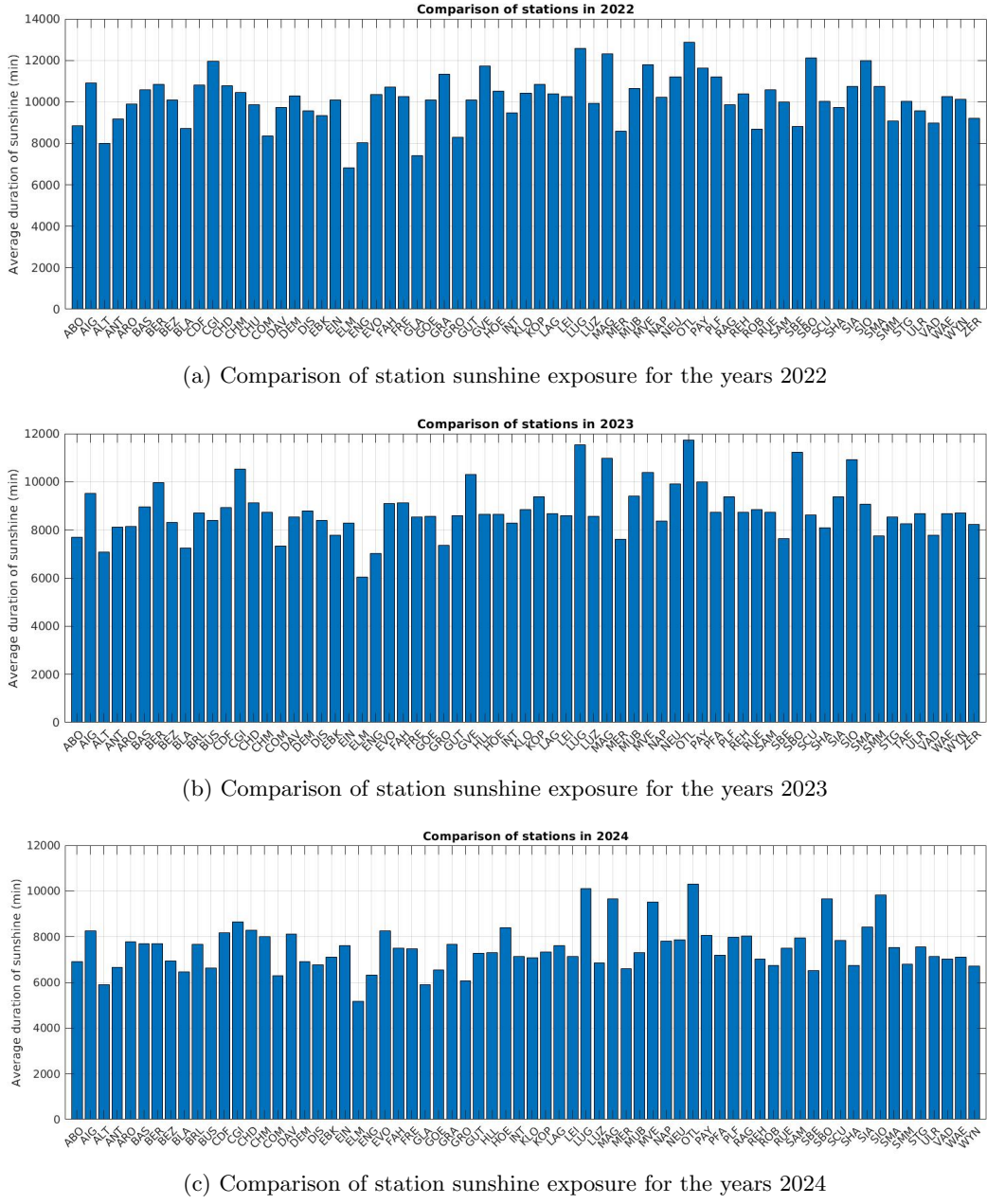


Figure 1: MATLAB-generated comparison of station sunshine exposure for the years 2022, 2023, and 2024 (in minutes).

The sunshine exposure in Locarno benefits from its favorable southern orientation, and located in southern Switzerland on Lake Maggiore, benefits from a Mediterranean-influenced climate characterized by higher average temperatures, significantly less cloud cover, and over 2,100 hours of sunshine annually. The geographical map used to illustrate these features (Figure 2) was generated using our MATLAB code. In order to better interpret the local characteristics shown on the map, additional background research was conducted, notably using Google Maps [12], to identify key landscape elements such as the surrounding mountains and the presence of Lake Maggiore.

The map also indicates an altitude of approximately 300 meters, which contributes to easy accessibility. To the rear of the station, a large mountain rises sharply: within just 3–4 km horizontally, the elevation increases to about 1,276 meters, reaching the Cimetta station (CIM). This steep gradient offers promising potential

for the installation of solar panels. In addition, the proximity of Lake Maggiore could represent a further advantage for solar energy production, as water surfaces may enhance solar irradiance through reflectance effects; however, this potential benefit remains hypothetical and would require a dedicated analysis.

Conversely, Elm is situated in a deep Alpine valley at about 960 meters altitude. Its southern exposure offers some sun, but its potential is severely limited by prolonged shading from high mountains—especially in winter when the sun is low—heavy cloud cover, substantial snowfall that can cover panels, and a much higher annual precipitation rate.

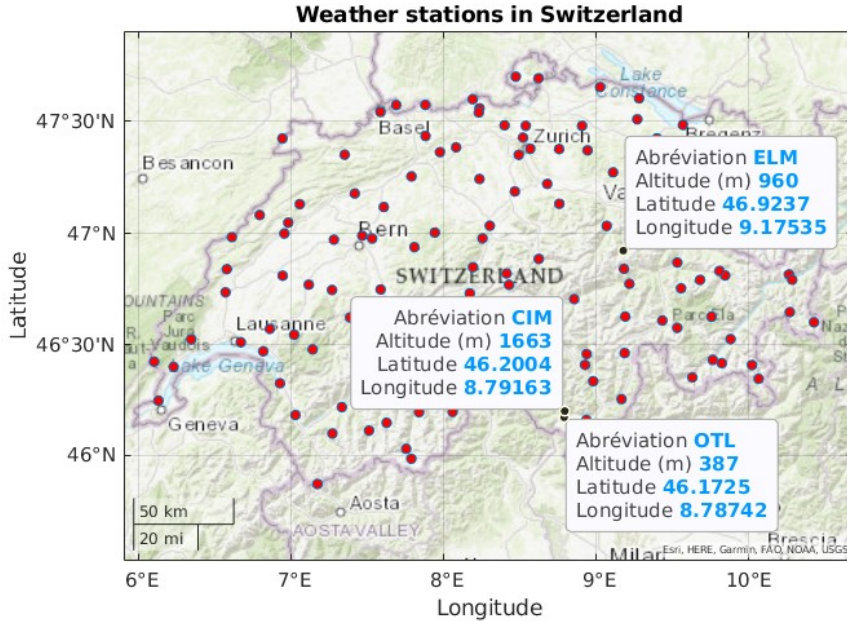


Figure 2: MATLAB-generated map of the three selected weather stations with elevation data.

## 5.2 Sunshine Stability and Optimal Trade-off

Figure 7a, Figure 7b and Figure 3c present the results of the sunshine stability analysis for the years 2022, 2023, and 2024, respectively. For each year, the MATLAB outputs display the five most stable stations based on the coefficient of variation (CV) of monthly sunshine duration, as well as the five best-performing stations according to the combined sunshine–stability trade-off metric.

Across the three years, the stability rankings show consistent patterns, with several stations repeatedly appearing among the lowest CV values like Locarno (OTL). This indicates that intra-annual sunshine stability is largely persistent over time and mainly driven by geographical and climatic factors rather than interannual variability.

The trade-off analysis highlights a different ranking compared to stability alone. Stations that combine relatively high annual sunshine duration with moderate seasonal variability tend to outperform stations that are either very stable but less sunny, or very sunny but strongly seasonal. As shown in the figures, this combined metric provides a more balanced assessment of photovoltaic site suitability.

Overall, these results confirm that sunshine stability constitutes a meaningful complement to total sunshine duration when comparing photovoltaic locations. Ensuring consistent sunshine throughout the year is essential for maintaining reliable and efficient photovoltaic electricity production.

Analysis for 2022 :

Top 5 most stable stations:

station_names	mean_min	std_min	cv
{'SBE'}	8824	2244.8	0.2544
{'SAM'}	9989.9	2829.1	0.2832
{'OTL'}	12887	3707.3	0.28767
{'ROB'}	8669.2	2577.9	0.29736
{'ZER'}	9206.1	2747.3	0.29842

Top 5 best trade-off stations (sunshine + stability):

station_names	mean_min	cv	score
{'OTL'}	12887	0.28767	44798
{'LUG'}	12568	0.31064	40458
{'SBO'}	12122	0.33788	35876
{'SAM'}	9989.9	0.2832	35276
{'MVE'}	11780	0.33626	35032

(a) Sunshine stability and trade-off ranking for 2022

Analysis for 2023 :

Top 5 most stable stations:

station_names	mean_min	std_min	cv
{'SBE'}	7648.7	1905.7	0.24915
{'SAM'}	8724.5	2211.5	0.25348
{'OTL'}	11726	3452.9	0.29448
{'COM'}	7333	2168.6	0.29573
{'LUG'}	11545	3448.4	0.29869

Top 5 best trade-off stations (sunshine + stability):

station_names	mean_min	cv	score
{'OTL'}	11726	0.29448	39819
{'LUG'}	11545	0.29869	38652
{'SBO'}	11232	0.30294	37077
{'SAM'}	8724.5	0.25348	34419
{'SBE'}	7648.7	0.24915	30699

(b) Sunshine stability and trade-off ranking for 2023

Analysis for 2024 :

Top 5 most stable stations:

station_names	mean_min	std_min	cv
{'DAV'}	8113.1	2324.7	0.28653
{'NAP'}	7806.5	2421.9	0.31024
{'MVE'}	9511.6	3201.4	0.33658
{'EVO'}	8245.8	2792.3	0.33864
{'ROB'}	6741.8	2288.9	0.3395

Top 5 best trade-off stations (sunshine + stability):

station_names	mean_min	cv	score
{'LUG'}	10096	0.34969	28871
{'OTL'}	10313	0.36191	28497
{'DAV'}	8113.1	0.28653	28315
{'MVE'}	9511.6	0.33658	28260
{'SBO'}	9663.3	0.36998	26119

(c) Sunshine stability and trade-off ranking for 2024

Figure 3: MATLAB-generated sunshine stability and trade-off rankings for the years 2022–2024.

### 5.3 Photovoltaic Cell Temperature

To model panel performance, we first computed the average photovoltaic cell temperature ( $T_{cell}$ ) for each month. The results (Figure 4) highlight a significant thermal contrast: during summer,  $T_{cell}$  in Locarno averages approximately 31°C, while in Elm it remains at a notably lower 22°C. These values include nighttime cooling, underscoring the substantial diurnal heating experienced during peak sunlight hours.

1 Abbreviation_station	2 Jan	3 Feb	4 Mar	5 Apr	6 May	7 Jun	8 Jul	9 Aug	10 Sep	11 Oct	12 Nov	13 Dec	14 Tcell_annual_mean
18 'EBK'	-1.4881	2.5769	6.2859	11.5384	20.1544	25.3185	26.8280	24.0422	14.2677	12.4540	5.4030	0.7792	12.3467
19 'EIN'	-2.0728	1.2291	6.4941	10.6978	18.8306	23.1702	25.1928	22.8426	13.1437	11.5139	4.1876	-0.0168	11.2677
20 'ELM'	-3.9277	-0.5514	4.9027	10.1649	16.7434	21.3739	22.5726	20.9136	12.1783	11.5412	3.6275	-1.1828	9.8630
21 'ENG'	-2.3560	0.6861	6.2302	10.1599	17.5739	22.0988	23.9152	20.9967	12.8490	11.6428	3.5770	-0.5498	10.5687
22 'EVO'	-1.8801	-1.2712	4.9445	9.1683	15.9314	20.2200	23.1096	20.6301	12.7206	9.9648	1.3223	-1.1998	9.4717
23 'FAH'	0.5036	3.8420	7.9629	11.2535	19.9676	24.1282	26.5516	25.5747	15.1528	13.5747	6.2395	1.9387	13.0575
24 'GRA'	0.3703	3.6877	8.0523	12.0279	21.0097	25.5691	27.2440	24.1895	15.2329	13.1106	6.5563	3.2463	13.3597
25 'GVE'	1.3211	4.5468	8.6487	13.5829	22.3985	26.9244	29.9722	27.4733	18.2749	14.7111	7.5430	4.3240	14.9767
26 'GLA'	-0.8511	2.6464	6.9075	11.5342	19.1851	23.6610	24.9423	22.9229	14.0311	12.1053	5.6473	1.5549	12.0239
27 'GOE'	1.5438	4.0890	8.0978	12.9642	22.1901	26.3680	28.4477	26.1186	16.0330	14.1738	7.3428	2.8437	14.1844
28 'GRO'	0.5124	3.7714	6.7446	13.0753	21.0389	24.8271	27.8826	26.1037	17.0429	13.6732	4.6417	-0.0649	13.2707
29 'GUT'	1.2044	3.9466	7.5464	12.7763	21.7740	26.0990	27.8624	25.5584	15.4328	12.8960	7.1042	2.6135	13.7362
30 'HOE'	-0.3441	1.1233	6.8632	8.8992	17.2707	21.4775	23.4049	21.8660	11.7384	12.9041	4.9706	0.8967	10.9225
31 'INT'	-0.9470	2.3121	7.2487	12.3975	20.3141	23.9386	26.1364	23.9328	15.4108	12.1736	5.1615	1.5491	12.4690
32 'KOP'	0.5198	3.3634	6.8996	11.6101	20.6316	24.5945	26.6502	24.5375	15.4394	13.0786	6.2428	2.2350	12.9835
33 'CDF'	-0.4243	2.0886	7.4871	10.2854	17.9913	23.5984	26.2177	23.5026	12.6828	12.5923	5.4312	1.6544	11.9256
34 'FRE'	-1.4906	0.0565	5.8787	8.2619	16.5823	21.1151	23.0299	21.1927	10.9690	11.2654	3.7349	0.4488	10.0870

Figure 4: Illustrative excerpt of the `Tcell_table` for the year 2022 (`Tcell_2022`) showing the 12 monthly  $T_{\text{cell}}$  values in  $^{\circ}\text{C}$  and the annual average for selected stations.

## 5.4 Panel Efficiency and Thermal Effects

The photovoltaic efficiency was computed for each station using the estimated mean cell temperature. Overall, efficiency variations between sites remain limited, typically ranging between 21% and 22%. This relatively narrow range reflects the moderate differences in annual average cell temperature across Switzerland.

However, the results highlight an important thermal effect: locations with higher solar exposure tend to exhibit higher operating temperatures, which negatively affect module efficiency due to the temperature sensitivity of crystalline silicon cells [6, 13]. Solar modules, which are generally dark-colored, absorb a large fraction of incident radiation, leading to significant heating during periods of high irradiance.

While efficiency losses remain moderate for cell temperatures around  $40^{\circ}\text{C}$ , they become increasingly pronounced at higher operating temperatures, typically above  $50\text{--}60^{\circ}\text{C}$  [6, 13]. As a consequence, higher irradiance does not necessarily translate into higher efficiency, even though it increases the total energy input.

These results indicate that efficiency alone is not a sufficiently discriminating parameter for site selection in this study. Instead, irradiance-related indicators, such as sunshine duration and plane-of-array energy yield, provide a more robust basis for comparing locations, while thermal effects should be considered as a secondary but non-negligible factor.

## 6 Conclusion and outlook

Based on the analysis conducted, Locarno emerges as the most favorable location for the installation of a photovoltaic park. This site combines high sunshine exposure, relatively stable seasonal variability, and favorable geographical conditions, making it well suited for large-scale photovoltaic deployment. In addition, its proximity to existing electrical infrastructure suggests that grid integration would be technically feasible, although a detailed connection study would be required to assess local capacity and operational constraints [14].

Although photovoltaic efficiency varies only marginally across the analyzed stations (approximately 21%–22%), the substantial differences in plane-of-array irradiance lead to significant variations in total energy production potential. Assuming a photovoltaic park surface of 2 hectares, the differences observed in plane-of-array irradiance between sites translate into substantial variations in total annual energy production, further reinforcing the dominant role of solar exposure in site selection. Under the climatic conditions considered, irradiance-related indicators therefore provide a more relevant basis for comparing locations than efficiency alone.

For future work, the analysis could be refined by incorporating additional site-specific factors such as terrain-induced shading, snow cover, and land-use constraints, as well as by exploring alternative system configurations including tracking systems or adjustable tilt angles. Despite these limitations, the present study provides a consistent framework for evaluating photovoltaic site potential in Switzerland using real meteorological data and established empirical models.

## 7 Authorship Statement

Contributor	Task
Perle	Implemented <code>function_clean_data</code>
Perle	Implemented <code>function_EPOA</code>
Perle	Implemented <code>function_Tcell</code>
Perle	Linked C and MATLAB code
Agathe	Wrote MATLAB code to display the station map
Agathe	Implemented code to calculate the sunniest stations
Agathe	Created the GitHub repository
Agathe	Wrote the C code
Both	Improved code readability and comprehensibility
Both	Wrote the project proposal
Both	Wrote the final report

Table 2: Detailed contributions by team members

## References

- [1] EPFL, *Energy Transition – Challenges and Opportunities*, course material, Moodle EPFL. [Online]. Available: <https://moodle.epfl.ch/course/view.php?id=19054> [Accessed Nov. 2025].
- [2] ScienceDirect, "A review on life cycle environmental impacts of emerging solar cells," 2024. [Online]. Available: <https://www.sciencedirect.com/science/article/pii/S0048969723066469> [Accessed Nov. 2025].
- [3] Swissolar, "Application du photovoltaïque – orientation et inclinaison optimales," 2024. [Online]. Available: <https://www.swissolar.ch/fr/connaissances/technologies-solaires/photovoltaïque/application> [Accessed Dec. 2025].
- [4] MeteoSuisse, "Open-source meteorological data," 2025. [Online]. Available: <https://www.meteosuisse.admin.ch> [Accessed Nov. 2025].
- [5] Sandia National Laboratories, "Photovoltaic performance modeling guide," PV Performance Modeling Collaborative, 2025. [Online]. Available: <https://pvpmc.sandia.gov/modeling-guide/> [Accessed Nov. 2025].
- [6] Sandia National Laboratories, "Faiman module temperature model," PV Performance Modeling Collaborative, 2025. [Online]. Available: <https://pvpmc.sandia.gov/modeling-guide/2-dc-module-iv/module-temperature/faiman-module-temperature-model/> [Accessed Nov. 2025].
- [7] Sandia National Laboratories, "PVLib MATLAB functions for photovoltaic modeling," GitHub repository, 2025. [Online]. Available: [https://github.com/sandialabs/MATLAB\\_PV\\_LIB/releases](https://github.com/sandialabs/MATLAB_PV_LIB/releases) [Accessed Nov. 2025].
- [8] Photovoltaïque.info, "Useful formula to find the reference yield," 2024. [Online]. Available: <https://www.photovoltaïque.info/fr/realiser-une-installation/choix-du-materiel/larchitecture-electrique/rendement-dun-systeme-photovoltaïque/> [Accessed Nov. 2025].
- [9] Engie MyPower, "Typical yield values for various PV technologies," 2023. [Online]. Available: <https://mypower.engie.fr/conseils/energie-solaire/production-energie-solaire/rendement-panneau-solaire.html> [Accessed Nov. 2025].
- [10] Sandia National Laboratories, *Photovoltaic Performance Modeling Fundamentals*, PV Performance Modeling Collaborative, 2025. [Online]. Available: <https://pvpmc.sandia.gov/modeling-guide/> [Accessed Nov. 2025].

- [11] A. P. Dobos, "PVWatts Version 5 Manual," National Renewable Energy Laboratory (NREL), Tech. Rep. NREL/TP-6A20-62641, Sep. 2014. [Online]. Available: <https://www.nrel.gov/docs/fy14osti/62641.pdf> [Accessed Dec. 2025].
- [12] Google Maps, "Switzerland," [Online]. Available: <https://www.google.com/maps> [Accessed Dec. 2025].
- [13] Tuco Énergie, "The impact of temperature on the efficiency of solar panels," [Online]. Available: <https://www.tucoenergie.fr/univers/impact-temperature-panneau-solaire> [Accessed Dec. 2025].
- [14] Swissgrid AG, "Swiss power grid," [Online]. Available: <https://www.swissgrid.ch/fr/home/operation/power-grid/swiss-power-grid.html> [Accessed Dec. 2025].
- [15] PVPRO, "Les différents types de panneaux solaires : avantages et inconvénients," [Online]. Available: <https://pvpro.fr/les-different-types-de-panneaux-solaires-avantages-et-inconvenients> [Accessed Dec. 2025].

## Appendices

### A Structure of the Input Data

This appendix provides an illustrative excerpt of the raw meteorological data used in this project. The objective is to show the structure and format of the input CSV files rather than the full dataset.

	reference_tir	tre200m0	tre200mx	tre200mn	tre005m0	tre005mn	tre005mx	ure200m0	pva200m0	prestam0	pp0qffm0	
AIG	01.01.2024 0 3.6	14.6	-5.2	2.5	-8.6	16.7		81 6.5		975.4	1022.3	
AIG	01.02.2024 0 6.6	13.9	-1.6	5.8	-4.8	19.7		78.4	7.6	971.3	1017.4	
AIG	01.03.2024 0 9.1	20.4		-2 8.4	-5.6			24 70.9		8 965.2	1010.6	
AIG	01.04.2024 0 10.6	26.5	-1.2	10.5	-4.6	30.3		67.9	8.6	971.9	1017.3	
AIG	01.05.2024 0	14	23	4 14.5	0.5	30.4			78 12.4	969.2	1013.9	
AIG	01.06.2024 0 18.5	29.5	8.3	19.1	5.9	35.6		74.5	15.7		970 1014.1	
AIG	01.07.2024 0 20.7	30.7	11.1	21.6	8.5	36.9		74.7	17.9	971.5	1015.2	
AIG	01.08.2024 0 21.1	30.6	11.9	21.8	9.7			36 76.1	18.7	971.7	1015.4	
AIG	01.09.2024 0 14.5	27.8	3.5	14.4	0.1	33.4			82 13.7	971.1	1015.8	
AIG	01.10.2024 0 12.3	22.7		2	12 -1.9	27.6		85.2	12.2	972.7	1017.9	
AIG	01.11.2024 0 6.1	14.8		-3 5.3		-6 18.6		81.3	7.7	977.3	1023.7	
AIG	01.12.2024 0 2.3	11.1	-4.2	1.2	-7.7	14.1		83.8	6.1	979.2	1026.4	
AIG	01.01.2025 0 3.4	15.4	-5.7	2.4	-9.5			18 79.8	6.3	973.1	1019.9	
AIG	01.02.2025 0 3.9	12.9	-3.7	3.2	-7.4	17.8			83 6.8	977.5	1024.3	
AIG	01.03.2025 0 8.2	21.2	-3.2	7.6	-6.9	23.1		68.5	7.2	969.5	1015.2	
AIG	01.04.2025 0 11.4	23.4	-0.5	11.5	-3.4	27.5		71.4	9.5	970.3	1015.5	
AIG	01.05.2025 0 11.1	22.0		11.0						971.0	1016.0	

Figure 5: Illustrative extract from the monthly raw meteorological data in CSV format provided by MétéoSuisse for the AIG (Aigle) station, showing the station metadata and certain meteorological variables. Only some of the available columns and rows are displayed for clarity.

### B Example of the EPOA\_table Structure

This appendix provides an illustrative extract of the **EPOA\_table** generated in this study. The table contains the monthly plane-of-array irradiance ( $E_{POA}$ ) values and the corresponding annual average computed for each meteorological station. The excerpt does not include the full dataset.

EPOA_2024 ×																
	Abbreviation_station	1	2	3	4	5	6	7	8	9	10	11	12	13	14	EPOA_annual_mean
1	'COM'	6 9139	9 2597	12 4698	61 3804	33 2160	67 0108	100 5716	86 1301	15 0625	8 1486	8 6424	5 9262	34 5610		
2	'ABO'	7 2843	11 8524	16 0502	75 4925	74 4584	94 2757	116 2948	109 5089	16 9144	10 9882	9 8770	6 9139	44 9917		
3	'AIG'	5 0620	9 6301	13 4575	45 4384	53 0379	84 2757	120 7400	103 6558	15 6798	9 8770	7 7782	4 9385	39 4642		
4	'ALT'	5 4324	9 7536	14 4452	56 6806	78 4973	90 6166	108 7991	90 6166	17 0379	9 0128	6 5435	3 7039	40 9283		
5	'ANT'	8 2720	11 9759	17 2848	105 1574	98 9874	108 0832	124 3779	114 9808	17 0379	10 2474	9 3832	6 0497	52 6531		
6	'ARO'	8 2720	11 8524	19 9453	95 7313	77 5019	88 8472	112 9705	105 1574	17 2848	10 7413	6 7905	47 1530			
7	'RAG'	6 1731	9 7536	15 1859	65 9059	95 7313	98 1845	119 4933	107 3612	17 0379	10 1240	9 1363	5 1854	46 6060		
8	'BAS'	5 4324	8 5189	14 8155	44 1300	85 2073	100 5716	121 9692	121 9692	17 1613	9 8770	6 6670	4 6916	45 0843		
9	'BER'	5 9262	10 2474	15 1859	62 5278	92 3532	108 0832	130 7030	118 2282	17 4083	10 2474	6 5435	4 5681	48 5019		
10	'BEZ'	5 0620	9 1363	13 9513	50 5519	87 9500	101 3530	122 5775	110 9108	17 1613	8 5189	5 0620	4 0743	44 6924		
11	'BLA'	5 5558	9 7536	14 5686	83 3352	89 7360	102 1275	137 7462	110 9108	15 3084	9 7536	6 4201	3 5804	49 0664		
12	'BUS'	5 3089	9 3832	13 4575	50 5519	81 4275	94 0579	115 6404	113 6460	16 1736	7 9016	4 6916	3 5804	42 9850		
13	'CHD'	7 4078	11 8524	15 8032	72 3808	70 2633	103 6558	133 4576	118 8631	16 9144	11 8524	9 8770	6 6670	48 2496		
14	'CHM'	6 4201	9 5066	14 8155	54 2635	72 3808	90 6166	124 3779	120 1189	15 9267	11 2351	9 2597	5 5558	44 5398		

Figure 6: Illustrative excerpt of the **EPOA\_table** for the year 2024 showing the 12 monthly  $E_{POA}$  values ( $\text{kWh m}^{-2} \text{month}^{-1}$ ) and the annual average for selected stations.

### C Photovoltaic Technologies Overview

This appendix provides a detailed overview of the main modern photovoltaic technologies used in commercial and industrial applications. The table below summarizes efficiency, advantages, and typical use cases [15].

Technology	Efficiency	Notes (Advantages and Limitations)
Monocrystalline Silicon (PERC / TOPCon)	18–24%	<b>Advantages:</b> Highest commercial efficiency; excellent low-light performance; long lifetime; good temperature behaviour. <b>Limitations:</b> Higher production cost than polycrystalline; slight performance loss in high heat.
Polycrystalline Silicon	13–18%	<b>Advantages:</b> Lower manufacturing cost; robust and mature technology. <b>Limitations:</b> Lower efficiency; gradually phased out in new installations.
Amorphous Silicon (a-Si)	6–9%	<b>Advantages:</b> Performs well under diffuse light and partial shading; lightweight and flexible possibilities. <b>Limitations:</b> Low efficiency; higher degradation (Staebler–Wronski effect).
HJT (Heterojunction) / Tandem (Perovskite–Si)	25–28%	<b>Advantages:</b> Cutting-edge high-efficiency technologies; low temperature coefficient; very strong bifacial potential (HJT). <b>Limitations:</b> Higher cost; tandem technologies not yet widely commercialised.
Thin-film (CdTe, CIGS)	10–17%	<b>Advantages:</b> Lightweight; good performance at high temperatures and in diffuse irradiance; flexible formats possible. <b>Limitations:</b> Lower yield per surface area; limited suppliers; environmental concerns for CdTe.

Table 3: Overview of common photovoltaic technologies with advantages and limitations

Monocrystalline silicon modules were selected for this study because they currently dominate the total solar photovoltaic cell market [2]. Their high efficiency (typically 18–24%) allows a more realistic representation of modern PV installations, particularly in utility-scale and industrial contexts. Furthermore, their good low-light performance, low degradation rate, and favourable temperature coefficients are consistent with the climatic conditions encountered across Switzerland, including Alpine and pre-Alpine regions.

Using monocrystalline technology therefore ensures that the simulated PV behaviour reflects the majority of real installations deployed today, increasing both the representativeness and the reliability of the yield estimations.

## D Station Abbreviations and Full Names

The following table lists all stations used in the analysis, with their MeteoSwiss abbreviations and full location names.

Table 4: Abbreviations and corresponding MeteoSwiss station names

Abr	Station Name	Abr	Station Name
COM	Comprovasco	ABO	Abojen
AIG	Aigle	ALT	Altenrhein
ANT	Antenen	ARO	Arosa
RAG	Rapperswil-Jona (Rapperswil SG)	BAS	Basel-Binningen
BER	Bern-Zollikofen	BEZ	Beznau
BLA	Blatten (Lötschental)	BUS	Büsserach
CHD	Château-d'Oex	CHM	Chaumont
DAV	Davos	DEM	Demaintse
DIS	Disentis	EBK	Ebenalp
EIN	Einsiedeln	ELM	Elm
ENG	Engelberg	EVO	Evolène
FAH	Fahy	GRA	Grächen
GLA	Glarus	GOE	Göschenen
GRO	Grosswangen	GUT	Guttannen
HLL	Hallau	HOE	Hoher Kasten
INT	Interlaken	KOP	Koppigen
BRL	Bièvre-La Cure (Bassins/Bière area)	CDF	Col du Grand St-Bernard
FRE	Fribourg	LAG	Langnau i.E.
LEI	Leirhnúkur (likely Leysin)	OTL	Locarno-Monti
LUG	Lugano	LUZ	Luzern
MAG	Magadino	MER	Meringen
MVE	Mühleberg (Müve)	MUB	Mühleberg Bözingen
NAP	Napf	NEU	Neuchâtel
CGI	Col du Grimsel	PAY	Payerne
PFA	Pfaffnau	PLF	Plaffeien
ROB	Robiei	RUE	Rünenberg
SBE	Schaffhausen-Beringen	SAM	Samnaun
SHA	Schaffhausen	SCU	Scuol
SIA	Sion-Airport	SIO	Sion
STG	St. Gallen	SMM	Saas-Maria / Marmorera
SBO	Samedan-Bever	ULR	Ulrichen
VAD	Vaduz	WAE	Wädenswil
WYN	Wynigen	REH	Rehetobel
SMA	S. Maria Val Müstair	KLO	Kloten-Zurich Airport

## E Maps for the Photovoltaic Panel Location

The following maps provide a visual representation of the proposed location for the photovoltaic panel installation situated behind the city of Locarno.



(a) Map showing city names and elevation contour lines



(b) Topographic map of the terrain